JOURNAL OF AIRCRAFT
Vol. 30, No. 5, Sept.–Oct. 1993

Computational Effects of Inlet Representation on Powered Hypersonic, Airbreathing Models

Lawrence D. Huebner*
NASA Langley Research Center, Hampton, Virginia 23665
and
Kenneth E. Tatum†
Lockheed Engineering and Sciences Co., Hampton, Virginia 23666

Computational results are presented to illustrate the powered aftbody effects of representing the scramjet inlet on a generic hypersonic vehicle with a fairing, to divert the external flow, as compared to an operating flow-through scramjet inlet. This study is pertinent to the ground testing of hypersonic, airbreathing models employing scramjet exhaust flow simulation in typical small-scale hypersonic wind tunnels. The comparison of aftbody effects due to inlet representation is well-suited for computational study, since small model size typically precludes the ability to ingest flow into the inlet and perform exhaust simulation at the same time. Two-dimensional analysis indicates that, although flowfield differences exist for the two types of inlet representations, little, if any, difference in surface aftbody characteristics is caused by fairing over the inlet.

Nomenclature

$\log [(\text{rms}_{\text{iter}})/(\text{rms}_1)]$	=	order of magnitude reduction in the computational residual
M	=	Mach number
p	=	pressure, psi
Re	=	Reynolds number
SNPR	=	static nozzle pressure ratio, p_3/p_∞
T	=	temperature, °F
u	=	x component of velocity, ft/s
X	=	streamwise distance from the nose, positive aft, in.
y^+	=	inner law variable, $\sqrt{\rho_1 u_1 \Delta z_1/\mu_1}$
Δz	=	normal point spacing in grid, ft
μ	=	viscosity, slugs/ft s
ρ	=	density, slugs/ft^3
Subscripts		
jet	=	conditions at nozzle throat
t	=	total conditions
wall	=	conditions at the body surface
1	=	conditions at first cell center away from the body surface
3	=	conditions at the combustor exit (see Fig. 1)
∞	=	freestream conditions

Introduction

HYPERSONIC airbreathing vehicles, such as the National Aero-Space Plane (NASP), utilize a supersonic combustion ramjet (scramjet) propulsion system. The location of this scramjet on the underside of the airframe and the shaping of the forebody and aftbody are prime concerns of propulsion/airframe integration (PAI) to provide optimum aeropropulsive performance. The forebody acts as part of the compression region for the inlet where the objective is to deliver a high-quality compressed flow to the scramjet inlet while maintaining low values for forebody drag. The aftbody serves as part of the external scramjet nozzle expansion for the exhaust gases and provides significant force and moment components for the entire vehicle. Therefore, the design of these types of vehicles is largely driven by the necessity of efficient PAI.[1]

The aerodynamic analysis and testing of such hypersonic, airbreathing vehicles under powered conditions is an important facet of PAI. Wind-tunnel testing of powered hypersonic, airbreathing configurations is both difficult and expensive due to the high temperatures and pressures necessary to sustain the hydrogen/air combustion process.[2] Also, size limitations of ground-based facilities preclude duplication of scramjet operation because the combustion process is not geometrically scalable.[2] Furthermore, computational solutions of the hydrogen/air combustion process is expensive, being feasible only with the most powerful supercomputers. In order to obtain powered data and avoid these problems, an experimental technique for the cold gas simulation of a scramjet exhaust was developed under NASA contract as part of the X-24C program in the mid-1970s.[3–5] The initial objectives of this study were to establish the standards of similitude for a hydrogen/air scramjet exhaust interacting with a hypersonic vehicle aftbody and to identify suitable gas mixtures which could be used to simulate scramjet exhaust in conventional wind tunnels. In this study, a mixture of argon and freon was identified as a suitable exhaust gas and was studied in addition to air. The objectives of this study were achieved, and the technique was adopted to support NASP technology development in the NASA Langley Research Center 20-Inch Mach 6 Wind Tunnel. This facility is described in Ref. 6. To date, two different hypersonic configurations and a simple aftbody model with a two-dimensional internal nozzle have been tested in this facility using the simulant gas technique.

A difficulty in the testing of powered hypersonic, airbreathing vehicles in this manner is that, since the models are limited in size by typically small hypersonic wind tunnels, it is impractical to test a powered model with both an operating flow-through inlet and scramjet exhaust flow simulation. One approach is to simply fair over the scramjet inlet and divert the flow around it. However, the flow path around the faired-over inlet will result in flowfields that are significantly differ-

Received Sept. 9, 1991; revision received April 23, 1992; accepted for publication April 23, 1992. Copyright © 1991 by the American Institute of Aeronautics and Astronautics, Inc. No copyright is asserted in the United States under Title 17, U.S. Code. The U.S. Government has a royalty-free license to exercise all rights under the copyright claimed herein for Governmental purposes. All other rights are reserved by the copyright owner.

*Aerospace Engineer, Hypersonics Group Leader, Supersonic/Hypersonic Aerodynamics Branch, Applied Aerodynamics Division, M/S 413. Senior Member AIAA.

†Principal Engineer, M/S 413, NASA Langley Research Center. Member AIAA.

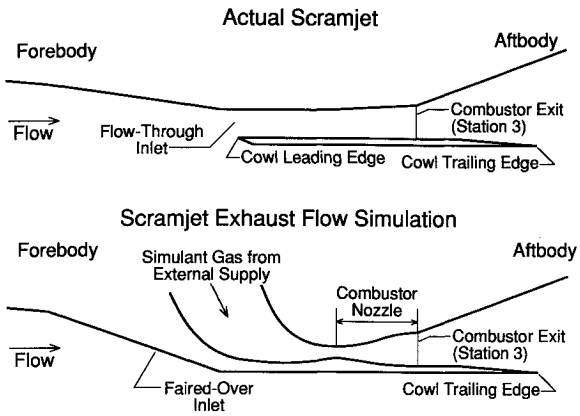

Fig. 1 Comparison of actual scramjet and scramjet exhaust flow simulation for powered testing.

ent from those past operating inlets and could possibly affect the external nozzle performance. Figure 1 shows the geometric differences in using scramjet exhaust flow simulation instead of actual scramjet combustion, and a faired-over inlet compared with a flow-through inlet. For the actual scramjet, flow into the engines is compressed by the forebody and the sidewalls of any inlet struts. The cowl leading edge isolates this captured internal flow from the external flow. The internal flow then passes the hydrogen injectors (not shown), combustion occurs, and the combustion products expand into the aftbody flowfield from the combustor exit (also referred to as station 3) over the nozzle/aftbody to the end of the configuration. For the scramjet exhaust flow simulation, the flowing inlet is faired over to allow the simulant gas to be routed into the model. The gas passes through a plenum, into the combustor nozzle designed for the simulant gas to provide inviscid similitude of the actual hydrogen/air combustion process at the combustor exit, and then expands into the aftbody flowfield. An analysis of the effects that different inlet representations have on aftbody flowfields lends itself well to the use of computational fluid dynamics (CFD).

This study on hypersonic, airbreathing configurations with scramjet exhaust flow simulation (hereafter referred to as "powered") is a two-dimensional computational effort to identify the effect of inlet representation on aftbody nozzle flowfields for a powered hypersonic airbreather (PHA) model. The approach taken was to examine the difference on aftbody flowfields and surface pressures for an operating flow-through scramjet inlet, and a faired-over inlet at a variety of freestream conditions.

Computational Method

The CFD code applied to the configurations of interest in this study is the General Aerodynamic Simulation Program (GASP).[7,8] GASP solves the integral form of the governing equations, including the full Reynolds-averaged Navier-Stokes equations, the thin-layer Navier-Stokes (TLNS) equations, the parabolized Navier-Stokes (PNS) equations, and the Euler equations. A generalized chemistry model and both equilibrium and nonequilibrium thermodynamics models are included as user options. The discretized equations may be solved by space marching or global iteration, and both explicit multistage Runge-Kutta and implicit time integration schemes are included. Characteristic-based spatial discretizations employ a variety of flux and Jacobian evaluation schemes. Computational efficiency is achieved through specialized memory management techniques for storage and input/output, as well as through a high degree of vectorization. GASP uses a multizonal algorithm that simplifies grid generation, but grid point connectivity is required along the zonal interface boundaries.

All viscous solutions assumed a laminar flow. For most of the computational flow conditions, this was a valid assumption. Further, Ref. 9 showed that there was little, if any, difference in surface pressures on the aftbody under powered conditions for laminar or turbulent flows. Also, the current study attempted to isolate the pure effects due to geometry differences in inlet representation. In the streamwise direction, full fluxes were employed with no splitting, using a Van Albeda-type smooth limiter and second-order, fully-upwind spatial discretization. In the spanwise (two-dimensional) and body-normal directions, Roe's flux difference splitting was employed using the Spekraize-Venkat limiter and third-order, upwind-biased spatial discretization.[8] First-order extrapolation boundary conditions were imposed in the two-dimensional, as well as at the outer grid boundary. No-slip, fixed-wall-temperature boundary conditions were imposed on all body surfaces, with $T_{wall} = 90°F$.

Before GASP (or any CFD code) can be used as an analysis tool, code calibration is essential for the types of flows of interest, providing a level of confidence in the ability of the code to accurately predict the fluid dynamics of the problem. Previous studies using this code have already shown that GASP has the ability to accurately predict complex three-dimensional hypersonic flows past configurations representative of NASP forebodies.[10-12]

Additional results have shown that GASP is capable of simulating the aftbody flows associated with powered hypersonic, airbreathing vehicles, lending credibility to GASP for this class of problem.[9,13] Reference 13 provides a qualitative comparison of powered-aftbody schlieren photographs with GASP solutions. Reference 9 provides quantitative comparison of GASP solutions with experimental data consisting of powered-aftbody surface and flowfield pressures. The significant conclusion from these referenced works, which is applicable here, is that viscous analysis is required for accurate determination of aftbody forces and moments, as well as aftbody flowfield features. In general, both studies confirmed the need for viscous solutions at a minimum to accurately predict the shocks emanating from the cowl trailing edge, propagation of cowl boundary layers into the shear layer, and boundary-layer displacement of aftbody shocks. Furthermore, TLNS solutions are required to predict any shocks produced by boundary-layer separation, such as might occur at the cowl trailing edge.

Effects of Inlet Representation on Aftbody Flows

In this section, the effects that the different inlet representations have on the aftbody are addressed computationally. These effects cannot be determined experimentally since the flow to the inlet cannot be evacuated at the same time a simulated combustion process is taking place within the nozzle. Figure 2 shows the two-dimensional PHA geometries used in the CFD analysis at the model symmetry plane. The PHA configuration has an initial forebody angle of 5 deg, followed by an additional compression of about 4 deg for the flow-through inlet representation. For the faired-over inlet, the fairing begins at the compression ramp break, and this second compression angle is about 10 deg larger than the initial forebody ramp angle. The cowl trailing edge is located about 21 in. behind the nose of the PHA. The initial nozzle expansion angle begins at the combustor exit and is approximately 19 deg and transitions midway down the aftbody to about 10 deg for the remainder of the expansion, ending at a distance approximately 33.5 in. from the nose. The bottom of Fig. 2 compares the geometry differences in the two inlet representations. This study examines configuration flowfields, aftbody surface pressures, and the integrated force and moment components of the aftbody nozzle to determine the impact of fairing over the inlet on the powered aftbody.

Computational Procedure

The computational grid information pertinent to CFD simulation of the PHA with both a flow-through and a faired-over inlet is shown in Fig. 3. Since the solutions are two-dimensional, the lower-surface centerline geometry in-

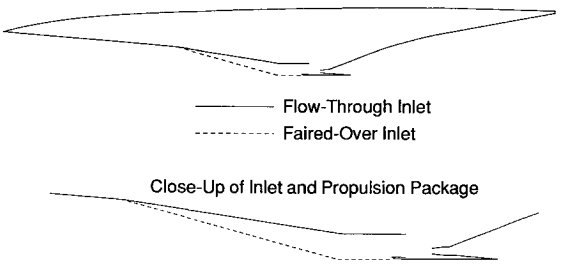

Fig. 2 Comparison of flow-through and faired-over inlet representations.

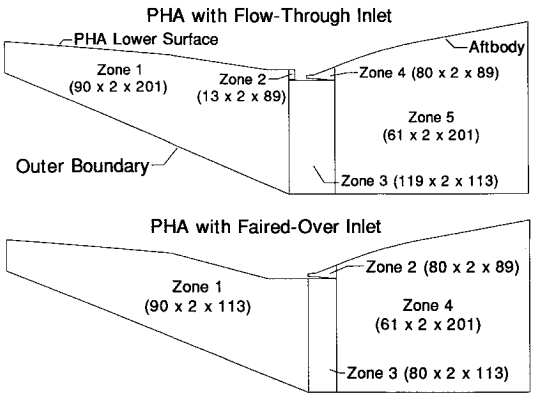

Fig. 3 Grid information for PHA CFD simulation.

formation is the only part of the configurations that is computationally modeled. Computationally, the external flow was initialized with constant freestream conditions at the nose, while the internal flow was initialized at the throat of the internal nozzle where the flow is assumed to be sonic with constant conditions spanning the nozzle height (i.e., no preset boundary layer). Since this effort only looked at the differences associated with different inlet representation and not actual aftbody performance, the perfect gas air assumption was modeled instead of the computationally more expensive scramjet-exhaust simulant gas. Both inviscid and viscous CFD solutions were obtained on the same grids. Due to the geometry of the lower surface of the PHA and the grid-point connectivitiy required by GASP, a logical choice was made to set up the flow-through inlet grid using five zones (Fig. 3, top) and the faired-over inlet using four zones (Fig. 3, bottom). The extra zone for the flow-through inlet configuration is the internal inlet zone, which extends only a short distance into the inlet. The internal inlet flow itself is not significant in this study, just the presence of an inlet, particularly including the cowl leading edge, from which the differences in the external flow are created. Grid dimensions are shown for each zone, and it should be noted that the grid points in the internal (nozzle) zone and the last (aftbody) zone were identical for body configurations. The grid points were clustered near the body to provide accurate resolution of the boundary layer for viscous calculations. The inner law variable y^+, provides a measure of accuracy of the viscous solutions by combining density, velocity, and viscosity with the amount of normal point spacing at the first computational cell center off the body. Typically, y^+ values on the order of one will provide adequate viscous resolution.[14] For this effort, values were less than two, except in the region where the boundary layer was beginning to develop (near the nose and just downstream of the nozzle throat).

Table 1 lists the conditions that were simulated on the flow-through and faired-over inlet PHA. These flow conditions represent two trends: 1) a variation in freestream Mach number at constant Reynolds number, and 2) a variation in Reynolds number at constant Mach number. As previously mentioned, the exhaust gas is assumed to be air modeled as a perfect gas. The internal (jet) conditions are initialized at the

Table 1 Computational flow conditions

M_∞	Re_∞, $\times 10^6$/ft	p_∞, psia	SNPR
2.0	2.0	1.178	4
3.0	2.0	0.419	12
4.0	1.9	0.158	31
6.0	0.5	0.019	256
6.0	1.0	0.032	154
6.0	2.0	0.063	77
6.0	4.0	0.139	35
6.0	7.0	0.260	19
10.14	1.8	0.030	160
14.0	2.0	0.022	223

nozzle throat with $M_{jet} = 1.0$, $p_{t,jet} = 30$ psia, and $T_{t,jet} = 100°F$. This yields an average static pressure at the combustor exit of 4.867 psia. Normalizing this by the freestream pressure for a specific case produces the values of static nozzle pressure ratio (SNPR) listed in the table. It should be emphasized that the variation in SNPR is due only to differences in freestream pressure for each condition since the internal flow parameters were fixed and identical for all cases.

Convergence and Numerical Accuracy Issues

Before presenting the effects of inlet representation on aftbody flows, convergence and numerical accuracy issues associated with the computational solutions are addressed. The issues to be highlighted are convergence histories for physical data, residual histories for TLNS solutions, and a comparison of computational models (Euler, PNS, and TLNS) for one set of input physical conditions.

One issue that arises when performing CFD calculations is how much to reduce the residual in order to obtain a correctly converged solution. Convergence histories of aftbody pressures were studied for PNS solutions of the flow-through and faired-over inlet PHA representations at $M_\infty = 6.0$, $Re_\infty = 2.0 \times 10^6$/ft, and SNPR = 77 as shown in Fig. 4. For both representations, one can see that very little physical difference in aftbody surface pressure is obtained by reducing the residual from four to five orders of magnitude; however, it requires about 50% more computational time to get that extra order-of-magnitude reduction. For this reason, a four order-of-magnitude reduction on each plane was prescribed for all subsequent Euler and PNS solutions.

Solutions were also computed on medium and coarse resolution grids having similar point clustering, but $\frac{3}{4}$ and $\frac{1}{2}$ the number of grid cells, respectively, in the streamwise and normal directions of the baseline (fine) grid. Forces computed on the medium grid varied by no more than 1.1% from those of the baseline grid. However, coarse grid results varied by up to 7% in lift compared to the baseline grid results. These results indicated that the fine grid resolution was adequate for the problem being considered, since further grid refinement would likely have changed the force and moment results by no more than 1%.

For high values of SNPR that cause the exhaust plume to propagate away from the body, the external flow is likely to be separated near the cowl trailing edge, thus a TLNS solution is required to accurately model the flows associated with it. One such condition of interest is for $M_\infty = 6.0$, $Re_\infty = 0.5 \times 10^6$/ft, and SNPR = 256. A laminar TLNS solution was computed on the faired-over inlet PHA at these conditions. One difference in a PNS vs a TLNS solution using GASP, is that for a PNS solution a residual reduction is imposed on each plane. On the other hand, a TLNS solution requires that a global residual reduction of the entire solution field be imposed. Therefore, instead of monitoring the number of iterations on a plane which are required to achieve the prescribed residual reduction, the progress of the solution is monitored by studying the residual reduction as a function of the number of global iterations. For this case, 1003 iterations were required to get a global residual reduction of four orders of

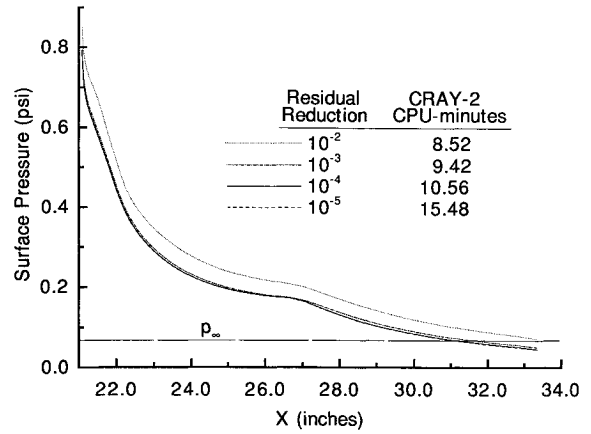

a) Flow-through inlet

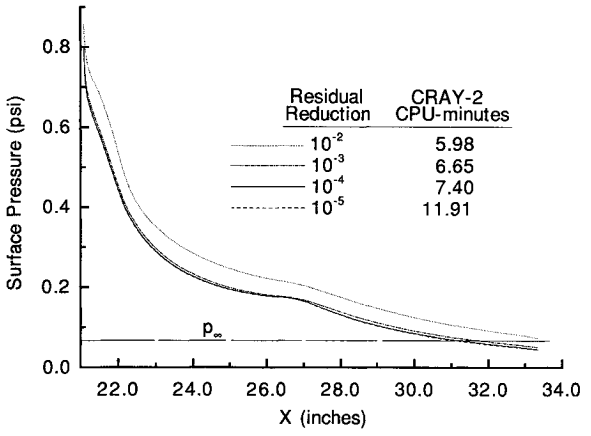

b) Faired-over inlet

Fig. 4 PNS aftbody surface pressure convergence histories, M_∞ = 6.0, Re_∞ = 2.0 × 10^6/ft, SNPR = 77.

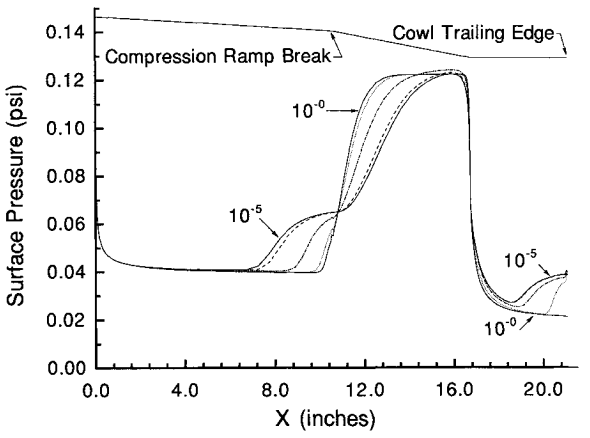

a) Forebody to cowl trailing edge

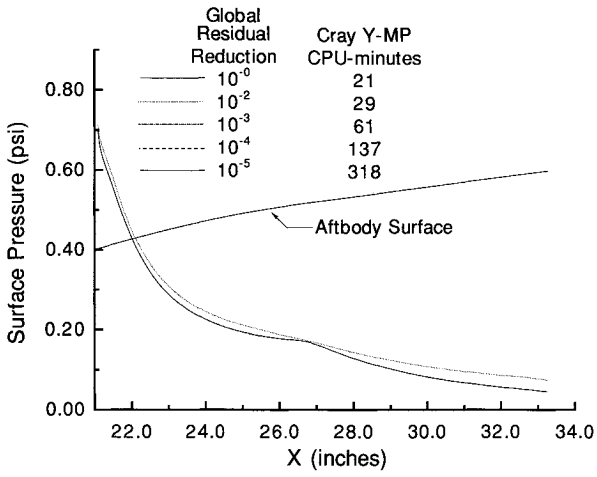

b) Aftbody

Fig. 5 Surface pressure convergence histories, TLNS faired-over inlet solution, M_∞ = 6.0, Re_∞ = 0.5 × 10^6/ft, SNPR = 256.

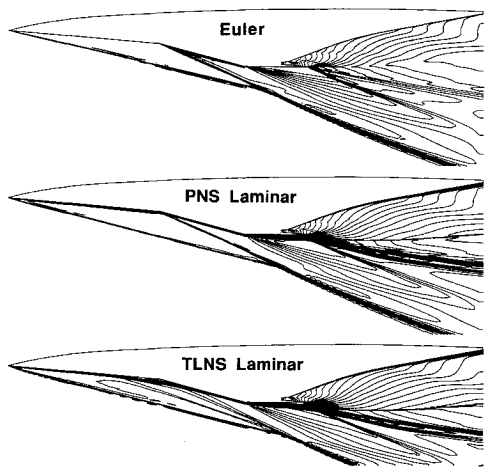

Fig. 6 Flowfield comparison of solutions with different computational models, PHA with faired-over inlet, isoMach lines, M_∞ = 6.0, Re_∞ = 0.5 × 10^6/ft, SNPR = 256.

magnitude, and an additional 866 iterations were required to reduce it by one more order of magnitude. Surface pressure convergence histories are shown in Fig. 5 for the forebody (from the nose to cowl trailing edge) and for the aftbody surface. On the forebody, the TLNS solution was initialized with a PNS marching solution which took 21 Cray Y-MP CPU-minutes to converge three orders of magnitude (the 10^{-0} solution on the figure). This initial (PNS) solution showed an increase in pressure at the compression ramp break, as well as a lack of separation predicted near the cowl trailing edge. Using the PNS solutions from the forebody and internal nozzle to initialize the aftbody flowfield at the cowl trailing edge, global TLNS iterations were then performed in all three zones. As the TLNS solution converged, the surface pressure histories indicated that separation occurred not only at the cowl trailing edge, but also at the compression ramp break. Furthermore, after reducing the global residual by two orders of magnitude, it took roughly twice as long to achieve each subsequent order-of-magnitude reduction. On the aftbody, there was no discernible difference in surface pressures once the global residual was reduced by three orders of magnitude.

A comparison of Euler, PNS, and TLNS solutions for this case is shown in Figs. 6 and 7. The Euler and PNS solutions were both converged to four orders of magnitude on each marching plane. Mach number contours (Fig. 6) show the flowfield differences in these solutions. The Euler solution predicts the location of the external shocks emanating from the nose, compression ramp break, and the cowl trailing edge, but does not predict the extent of the shear layer and the compression wave inside of the plume as do the two viscous solutions. Furthermore, the TLNS solution models the separated flow near the compression ramp break, as well as the separation at the cowl trailing edge with its weak separation shock. Despite these flowfield differences, the level of computational modeling seems to have little impact on the aftbody surface results, as shown in Fig. 7. The surface pressure differences are primarily restricted to the beginning of the aftbody, with only small variations further downstream. Even though there is a pressure difference in the two viscous solutions at the cowl trailing edge, the 0.10 psia difference is minimal and the trends are consistent downstream of that point. Furthermore, the TLNS solution showed a slightly larger boundary layer than the PNS solution at the combustor exit, and the details of the expansion beyond the combustor exit were different as well. A comparison of the aftbody lift, thrust

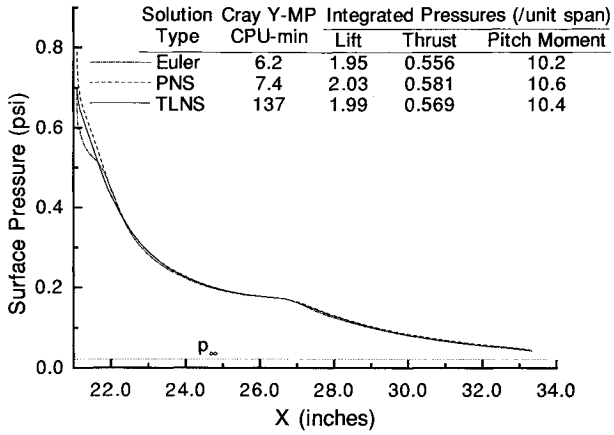

Fig. 7 Aftbody surface pressure comparison of solutions with different computational models, PHA with faired-over inlet, $M_\infty = 6.0$, $Re_\infty = 0.5 \times 10^6$/ft, SNPR = 256.

(both in pounds per unit span), and pitching moment (in inch-pounds per unit span) values shows only a 4% difference between the three solutions. It should be noted that the force and moment values for these and all subsequent solutions are obtained by integrating the differential pressures ($p - p_\infty$), and that the moment center was taken about the expansion corner of the combustor exit. Regardless of the minimal difference in aftbody surface pressures for this configuration for the three types of solutions, PNS solutions were obtained for the remainder of the simulation conditions of interest since the computational cost of obtaining the PNS solution was about the same as the Euler solution and almost $\frac{1}{20}$ of the TLNS solution. The average Cray Y-MP CPU time for these PNS solutions was 9 min for the faired-over inlet configuration, and 13 min for the flow-through inlet configuration.

Effect of Freestream Mach Number

To illustrate the complex flowfield associated with this type of CFD analysis, Fig. 8 shows a sketch of the salient flowfield features near the cowl for the flow-through inlet representation. Two forebody shocks are evident, a bow shock from the configuration nose and a forebody shock from the compression ramp break. A relatively strong shock from the cowl-leading edge exists, followed by an expansion and a recompression wave near the cowl. In the aftbody region, a shear layer between the internal plume region and the external flow is created by the propagation of the cowl inner and outer boundary layers. This expanding shear layer causes two more shocks to form, one inside the plume and the other outside the plume.

Figure 9 shows Mach number contour comparisons of the flow-through and faired-over inlet PHA at Mach numbers of 3.0, 6.0, and 14.0, and a Reynolds number of 2.0×10^6/ft. Comparing the two forms of inlet representation, significant differences are seen in the flowfields in the vicinity of the cowl. First of all, the cowl leading edge on the flow-through inlet creates a shock followed by a moderate expansion of the flow. Furthermore, there is a recompression of the flow between the expansion region and the cowl at the higher freestream Mach numbers. For the faired-over inlet, there is only an expansion at the corner that connects the fairing to the cowl. Secondly, the size of the boundary layer on the flow-through inlet cases is smaller because it develops only from the cowl leading edge instead of on the entire forebody, as in the faired-over inlet cases. In the aftbody region the flows are quite similar, including the locations of the cowl trailing-edge shock, the shear layer, and the weak shock wave between the shear layer and the aftbody.

The plume extent with increasing Mach number is related to the freestream pressure. As the Mach number increases at constant Reynolds number, the freestream pressure decreases. At $M_\infty = 3.0$, $p_\infty = 1.178$ psia, the external flow

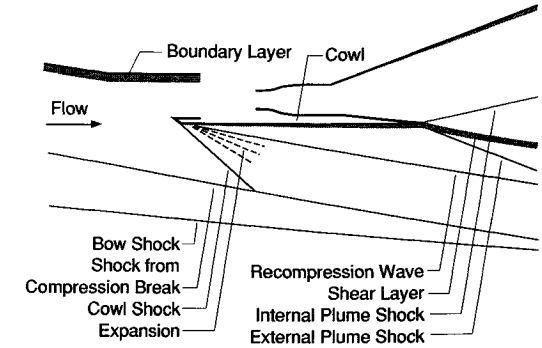

Fig. 8 Sketch of salient flowfield features near the cowl for the flow-through inlet representation.

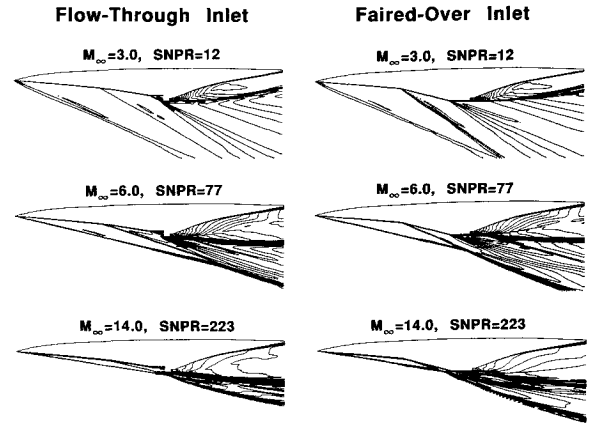

Fig. 9 Effect of Mach number on inlet representations, PHA isoMach lines, $Re_\infty = 2.0 \times 10^6$/ft.

dominates the aftbody flowfield and compresses the plume very near the aftbody surface. At $M_\infty = 14.0$, $p_\infty = 0.022$ psia, the plume accounts for a majority of the aftbody flowfield, so the shear layer and the external shock structures from the forebody and cowl leading edge are in much closer proximity.

Figure 10 presents comparisons of aftbody surface pressures and integrated force and moment components for the flow-through and faired-over inlets at the two extremes in Mach number and constant Reynolds number shown in the previous figure. Figure 10a shows the $M_\infty = 3.0$ solutions. The surface pressure distributions show small differences only near the trailing edge of the PHA which is likely due to the proximity of the plume to the aftbody. Furthermore, a comparison of the pressure integrations shows less than one-half of 1% difference in lift, thrust, and pitching moment. (Note that due to the high freestream pressure these are actually negative lift, drag, and nose-up pitching moment.) For the $M_\infty = 14.0$ condition (Fig. 10b), the integrated pressures again show little variance, amounting to integrated force and moment components of less than 1%, even though the external flow features are quite close to the plume, as shown in the previous figure. In this case, the freestream pressure is very low, producing the desired positive lift, thrust, and nose-down pitch moment. This trend of minimal differences in aftbody performance was observed in all freestream Mach numbers simulated.

Based on the very small differences in aftbody characteristics for the two inlet representations, Fig. 11 shows the Mach number effect (at nominal constant Reynolds number) for only the faired-over inlet case. It is evident that, except for the $M_\infty = 3.0$ case at high freestream pressure, the aftbody is affected very little by increasing Mach number. The integrated pressures vary due to the differences in freestream pressure for each case. Although there is a significant difference in the flowfields for the flow-through and faired-over inlets, the actual aftbody surface effects are quite small, due

to either inlet representation or to Mach number variation, except in the case of very low values of SNPR. It should be noted that scramjet operation is not expected at $M_\infty = 3.0$, but it does provide the extreme case for exercising the effect of inlet representation from a computational point of view.

Effect of Freestream Reynolds Number

Figure 12 shows Mach number contour comparisons of the flow-through and faired-over inlet PHA at $M_\infty = 6.0$ and Reynolds numbers of 0.5, 2.0, and 7.0 × 10⁶/ft. (The $M_\infty = 6.0$, $Re_\infty = 2.0 \times 10^6$/ft solution was previously shown in Fig. 9.) As expected, because of the variation in freestream pressure, similar differences in flowfield features exist between the two inlet representations as discussed in the previous section. Most importantly, there are only subtle differences in the magnitude of the contour levels within the plume. One can see very little difference in the positions of the bow shock and the shock from the compression ramp break with increasing Reynolds number for the two inlet representations. This is not surprising since the shock shape is primarily a function of Mach number. The relationship between plume extent and freestream pressure is also evident in this figure. For the low value of freestream pressure, the plume dominates the aftbody flowfield and decreases in size with increasing freestream pressure.

Figure 13 shows the aftbody surface characteristics at the two extremes in Reynolds number for the two inlet representations. At the low Reynolds number (low p_∞) there is no

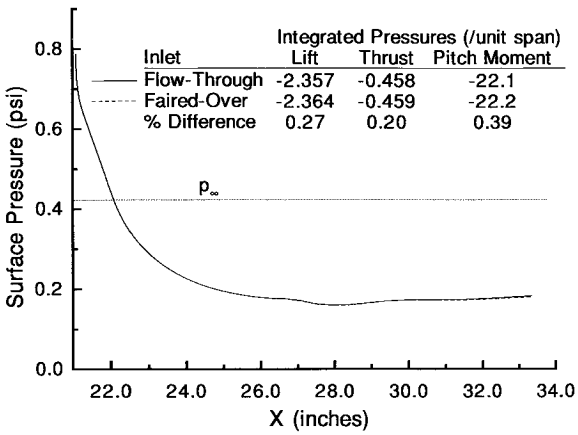

a) $M_\infty = 3.0$, SNPR = 12

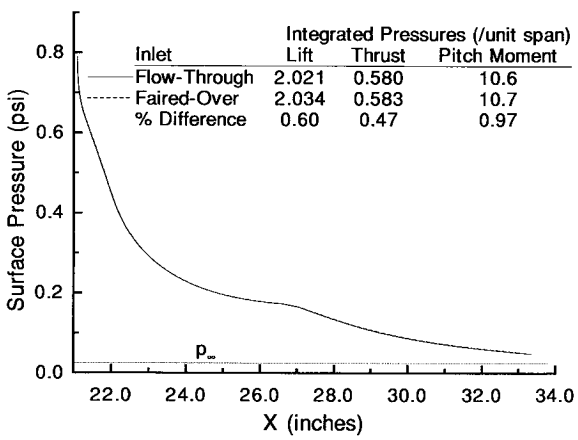

b) $M_\infty = 14.0$, SNPR = 223

Fig. 10 PNS aftbody surface pressures of flow-through and faired-over inlet representations, $Re_\infty = 2.0 \times 10^6$/ft.

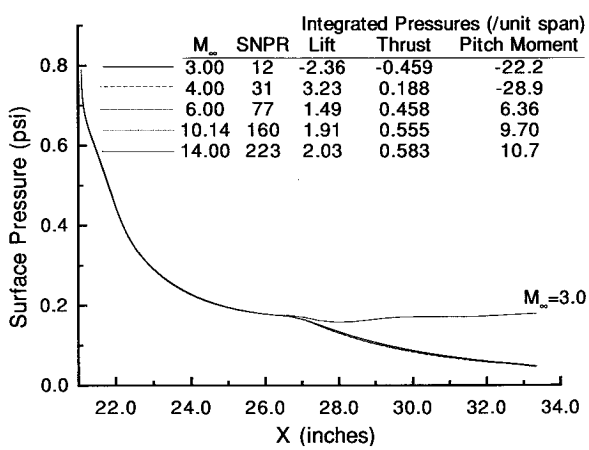

Fig. 11 Effect of Mach number on PNS aftbody surface pressures, PHA with faired-over inlet, $Re_\infty \cong 2.0 \times 10^6$/ft.

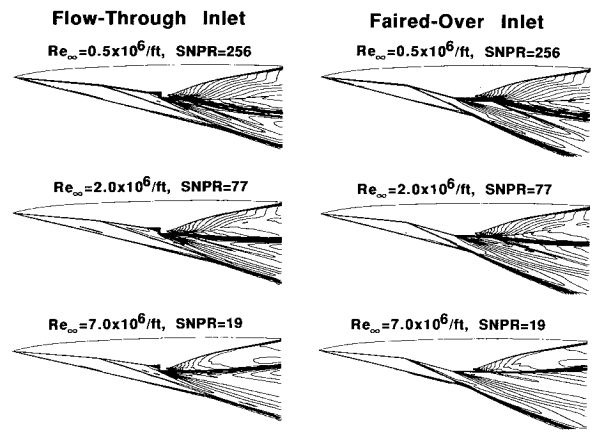

Fig. 12 Effect of Reynolds number on inlet representations, PHA isoMach lines, $M_\infty = 6.0$.

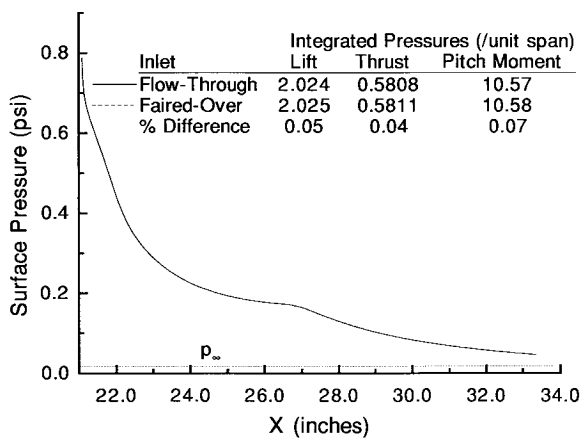

a) $Re_\infty = 0.5 \times 10^6$/ft, SNPR = 256

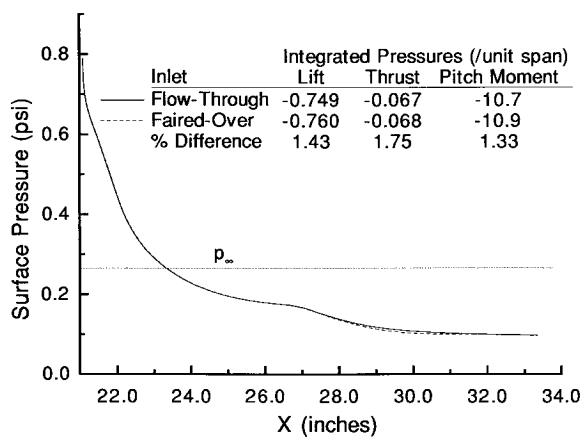

b) $Re_\infty = 7.0 \times 10^6$/ft, SNPR = 19

Fig. 13 PNS aftbody surface pressures of flow-through and faired-over inlet representations, $M_\infty = 6.0$.

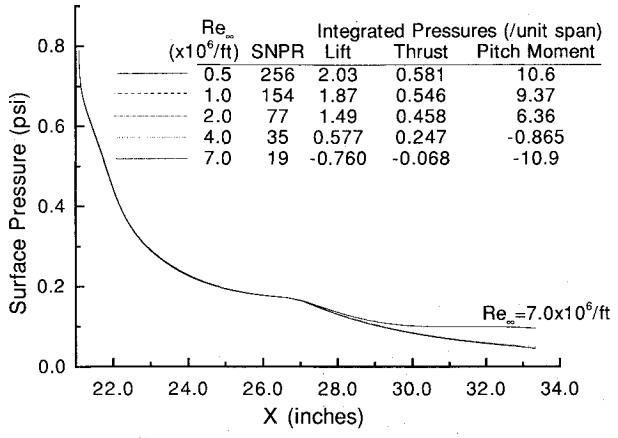

Fig. 14 Effect of Reynolds number on PNS aftbody surface pressures, PHA with faired-over inlet, $M_\infty = 6.0$.

difference in pressures or integrated pressures, and at the high Reynolds number (high p_∞) integrated pressure differences of less than 2% exist. As was the case in the Mach number variation, the effects on aftbody surface characteristics of the two inlet representations are only noticeable at the low SNPR (high Reynolds number) (Fig. 13b). Otherwise, no discernible differences were seen in inlet representation effects for the rest of the Reynolds number range.

Based on the very small differences in aftbody characteristics for the two inlet representations, Fig. 14 shows the Reynolds number effect (at constant Mach number) for just the faired-over inlet case. Except for the $Re_\infty = 7.0 \times 10^6$/ft case (high p_∞, low SNPR), the aftbody is affected very little by decreasing the Reynolds number. However, the integrated pressures again vary due to the differences in freestream pressure for each case. Once again, although there is a significant difference in the flowfields for the flow-through and faired-over inlets, the actual surface effects are quite small, due to either inlet representation or variation in Reynolds number, except in the case of very low values of SNPR.

Conclusions

Two-dimensional CFD analyses have been presented pertinent to the ground testing of hypersonic, airbreathing models employing scramjet exhaust flow simulation as it relates to propulsion/airframe integration.

The computational study just described indicates that there is little, if any, effect on aftbody surface characteristics due to representing the inlet with a fairing instead of with the flow-through inlet. The aftbody flowfield and surface characteristics are primarily dictated by the internal nozzle flow. Flowfield differences do exist because the flow-through inlet has a sharp cowl leading edge producing a lip shock, as opposed to the faired-over inlet where there is a simple expansion near the intersection of the fairing and the cowl. Through CFD analyses at various freestream Mach and Reynolds numbers, the variation of SNPR caused by p_∞ variation was shown to have no effect on aftbody surface pressures for values of SNPR greater than 40. Below this value, however, the plume remains close to the aftbody surface, and there is a small impact on aftbody surface pressures. Furthermore, there were indications that for cases with high values of freestream pressure (where the plume is closer to the aftbody) result, not in large differences between the two inlet solutions, but surface pressures that level off about half way down the aftbody instead of continuing to decrease as the internal flow expands into the aftbody flowfield.

It should be emphasized that these conclusions are based on two-dimensional CFD, which do not take into account three-dimensional lateral relief effects and the spanwise expansion of the plume onto any wing or control surfaces that may be subject to influence by the exhaust flow. Such effects may result in larger differences than have been shown herein. This may be particularly important if the aftbody contains flow-altering devices, such as a body flap or injectors for external nozzle burning.

References

[1]Edwards, C. L. W., Small, W. J., Weidner, J. P., and Johnston, P. J., "Studies of Scramjet/Airframe Integration Techniques for Hypersonic Aircraft," AIAA Paper 75-58, Jan. 1975.

[2]Hartill, W. R., "Method of Obtaining Aerodynamic Data on Hypersonic Configurations with Scramjet Exhaust Flow Simulation," NASA CR-2831, June 1977.

[3]Oman, R. A., Foreman, K. M., Leng, J., and Hopkins, H. B., "Simulation of Hypersonic Scramjet Exhaust," NASA CR-2494, March 1975.

[4]Hopkins, H. B., Konopka, W., and Leng, J., "Validation of Scramjet Exhaust Simulation Technique," NASA CR-2688, June 1976.

[5]Hopkins, H. B., Konopka, W., and Leng, J., "Validation of Scramjet Exhaust Simulation Technique at Mach 6," NASA CR-3003, March 1979.

[6]Keyes, J. W., "Force Testing Manual for the Langley 20-Inch Mach 6 Tunnel," NASA TM-74026, July 1977.

[7]Walters, R. W., Cinnella, P., Slack, D. C., and Halt, D., "Characteristic Based Algorithms for Flows in Thermo-Chemical Nonequilibrium," AIAA Paper 90-0393, Jan. 1990.

[8]Walters, R. W., Slack, D. C., Cinnella, P., Applebaum, M., and Frost, C., "A User's Guide to GASP, Revision 0," Virginia Polytechnic Inst. and State Univ., Blacksburg, VA, Nov. 1990.

[9]Tatum, K. E., Monta, W. J., Witte, D. W., and Walters, R. W., "Analysis of Generic Scramjet External Nozzle Flowfields Employing Simulant Gases," AIAA Paper 90-5242, Oct. 1990.

[10]Huebner, L. D., Pittman, J. L., and Dilley, A. D., "Hypersonic Parabolized Navier-Stokes Code Validation on a Sharp-Nose Cone," *Journal of Aircraft*, Vol. 26, No. 7, 1989, pp. 650–656.

[11]Haynes, D. A., Huebner, L. D., and Blair, A. B., Jr., "Computational Refinement of the LaRC Test Technique Demonstrator Forebody with Experimental Verification," *Sixth National Aerospace Plane Technology Symposium*, Paper No. 20, Monterey, CA, April 24–28, 1989, NASP CP-6034, Vol. I, pp. 27–46.

[12]Huebner, L. D., "Computational Investigation of LaRC Test Technique Demonstrator Reentry Configurations," *Seventh National Aero-Space Plane Technology Symposium*, Paper No. 36, Cleveland, OH, Oct. 23–27, 1989, NASP CP-7040, Vol. I, pp. 153–174.

[13]Huebner, L. D., and Tatum, K. E., "Computational and Experimental Aftbody Flowfields for Hypersonic, Airbreathing Configurations with Scramjet Exhaust Flow Simulation," AIAA Paper 91-1709, June 1991.

[14]Richardson, P. F., and Parlette, E. B., "Comparison Between Experimental and Numerical Results for a Research Hypersonic Aircraft," *Journal of Aircraft*, Vol. 27, No. 4, 1990, pp. 300–305.